

Soft Rasterizer: Differentiable Rendering for Unsupervised Single-View Mesh Reconstruction

Shichen Liu^{1,2}, Weikai Chen¹, Tianye Li^{1,2}, and Hao Li^{1,2,3}

¹USC Institute for Creative Technologies

²University of Southern California

³Pinscreen

{lshichen, wechen, tli}@ict.usc.edu hao@hao-li.com

Abstract

Rendering is the process of generating 2D images from 3D assets, simulated in a virtual environment, typically with a graphics pipeline. By inverting such renderer, one can think of a learning approach to predict a 3D shape from an input image. However, standard rendering pipelines involve a fundamental discretization step called rasterization, which prevents the rendering process to be differentiable, hence able to be learned. We present the first non-parametric and truly differentiable rasterizer based on silhouettes. Our method enables unsupervised learning for high-quality 3D mesh reconstruction from a single image. We call our framework “soft rasterizer” as it provides an accurate soft approximation of the standard rasterizer. The key idea is to fuse the probabilistic contributions of all mesh triangles with respect to the rendered pixels. When combined with a mesh generator in a deep neural network, our soft rasterizer is able to generate an approximated silhouette of the generated polygon mesh in the forward pass. The rendering loss is back-propagated to supervise the mesh generation without the need of 3D training data. Experimental results demonstrate that our approach significantly outperforms the state-of-the-art unsupervised techniques, both quantitatively and qualitatively. We also show that our soft rasterizer can achieve comparable results to the cutting-edge supervised learning method [49] and in various cases even better ones, especially for real-world data.

1. Introduction

We live in a complex three-dimensional world, consisting of limitless 3D shapes of objects and matter, and yet, our observations are only 2D projections of this world. One of the fundamental goals in computer vision, dating back to the

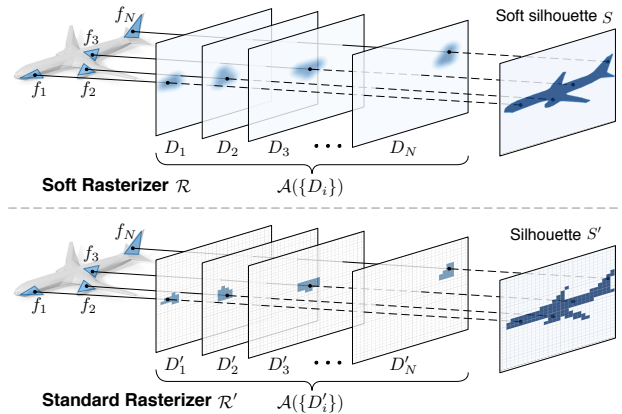


Figure 1: Our differentiable Soft Rasterizer \mathcal{R} (upper) can render mesh silhouette that faithfully approximates that generated by a standard rasterizer \mathcal{R}' (below). \mathcal{R}' renders a pixel as solid once it is covered by a projected triangle, leading to a discrete and non-differentiable process. We propose to approximate the rasterized triangles $\{D'_i\}$ with a “soft” continuous representation $\{D_i\}$ based on signed distance field. We further fuse $\{D_i\}$ with a differentiable aggregate function $A(\cdot)$, which is essentially a logical *or* operator, so that the entire framework is differentiable.

sixties [40], has been to build a computational system that can understand and reconstruct any 3D scenes, structures, and objects given a picture. Early attempts for single-view 3D modeling relied on hand-designed priors [28] or statistical models that describe the image formation process [30]. Later approaches include data-driven techniques that learn models from a collection of 3D data sets [14, 41].

Recent advancements of deep learning have shown that the computational gap between 2D images and scene analysis is closing for a wide range of end-to-end tasks using supervised learning, such as image recognition [13], object detection [37] and segmentation [24], *etc.* However, extend-

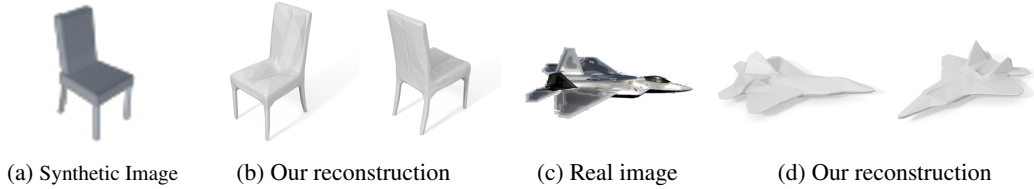


Figure 2: Example reconstruction results using our approach on testing synthetic image and real image.

ing the paradigm of supervised learning for 3D inference is non trivial, due to the limited availability of 3D assets compared to 2D images, as well as the complexity of rendering all possibilities w.r.t. shape, texture, lighting exhaustively. Consequentially, the ability to learn 3D deep models successfully without ground-truth supervision can lead to unprecedented possibilities for the general task of single-view 3D reconstruction tasks.

The key to unsupervised 3D inference is to find a way to relate the changes of non-domain specific 3D model parameters (e.g., geometry, illumination, material properties, *etc*) with those in the observed image. Differentiable rendering relates the derivatives of pixel intensities with the properties of the virtual object such that a 3D inference problem can be formulated by a gradient-based optimization without the need of supervised learning.

However, the rendering procedure is not differentiable in conventional graphics pipelines. In particular a 3D object is projected onto the 2D screen through a discretization step called *rasterization*, which is not differentiable, while the model projection itself is.

To enable unsupervised training for image-based reconstruction, a large body of work [39, 46, 45, 22, 9] have suggested various ways of approximating the rendering gradient computation in the backward pass. Most of the prior frameworks are designed for domain-specific purpose and remain difficult to handle more general cases. Recently, Kato et al. [19] have introduced the first general-purpose neural mesh renderer based on deep learning. In [19], they approximate the rasterization gradient with a hand-designed function which response is piecewise linear with respect to the displacement of vertices. While promising results were shown, the proposed linear function is too simplified to fully model the nonlinearity of a real rasterizer. Furthermore, their framework only approximates the backward gradient computation while directly using the standard rasterizer in the forward pass. The inconsistency between the forward and backward propagations makes it difficult to fully exploit the effectiveness of the rendering layer.

To address these issues, we propose the first *truly differentiable rasterizer* which is able to faithfully approximate the discrete rasterization in the forward pass of a deep neural network. Given a polygon mesh, our rasterizer can directly generate an approximated silhouette of the input un-

der a given view (Figure 1 upper). Our network is only trained with multi-view silhouettes. The difference between our rendered result and the true silhouette can be back propagated to the mesh generator, enabling unsupervised learning without 3D training data. At test time, our approach can reconstruct a high-quality 3D mesh from a single image.

The key insight of our work is that we show how to formulate the deterministic sampling operation of a rasterizer as a probabilistic procedure. While the standard rasterizer directly picks the color of the closest triangle in the viewing direction (Figure 1 below), we propose that all triangles have contributions to each rendered pixel with a certain probability. In particular, triangles which are closer to the projected pixels in screen space are more likely to be sampled from that pixel. To this end, we approximate the probabilistic contribution of each triangle face to the rendered pixels as a normalized distance field computed on the image plane (Figure 1 upper). By passing the collected distance field to a differentiable aggregate function $\mathcal{A}(\cdot)$, which simulates the logical *or* operator, our rasterizer can directly generate an approximated silhouette of the mesh. We call our framework *Soft Rasterizer (SoftRas)* as it is a soft approximation of the standard rasterizer.

SoftRas itself does not involve any trainable parameters and thus can serve as a flexible module for other applications. In addition, as we target for mesh reconstruction, our approach is able to generate higher quality results with much lower computational cost compared to techniques with voxel or point cloud based representations. Figure 2 shows examples of our model reconstructing a chair and fighter aircraft from a single image. We also show that our approach significantly outperforms existing unsupervised methods w.r.t. quantitative and qualitative measures. Furthermore, our experimental results indicate that our method can achieve comparable and in certain cases, even superior results to supervised solutions [49], indicating the effectiveness of the soft rasterizer framework.

2. Related Work

Differentiable Renderer. The standpoint of viewing vision problems as *inverse graphics* has been investigated since the very beginning of the field [3, 54, 34]. Through inverting the rendering progress, inverse graphics aims to infer the object shape, illumination and reflectance from an

image. To relate the changes in the observed image with that in the 3D model parameters, there are a number of existing techniques utilizing the derivatives of rendering.

Gkioulekas et al. [11] build a material dictionary and propose a direct optimization framework to invert volumetric scattering using stochastic gradient descent. In [10], researchers present an analytical formulation between the measurements and internal scattering parameters which enables a derivative-based optimization. Though the gradients are leveraged for solving the inverse problems, these approaches are limited to specific light transporting problems. Mansinghka et al. [29] propose a general inverse rendering technique by using a probabilistic graphics model to infer scene parameters from observations. More recently, Loper and Black [27] further introduce OpenDR, an approximate differentiable renderer which can be incorporated into probabilistic programming framework to obtain derivatives with respect to the model parameters.

With the recent surge of convolutional neural network, there is an increasing popularity to consider rendering derivatives in a deep learning framework. In particular, many learning-based techniques [57, 26, 39, 46, 45, 6, 22, 33, 9] have incorporated a *differentiable rendering layer* to enable an end-to-end architecture for 3D reconstruction and material inference in an unsupervised manner. However, these rendering layers are usually designed for special purpose and thus cannot be generalized to more general cases. Nalbach et al. [31] propose a general deep shading network which learns the direct mapping from a variety of deferred shading buffers to corresponding shaded images. Rezende et al. [38] pioneer in unsupervised 3D structure generation from a single image using a differentiable renderer. Later, a differentiable rendering pipeline specialized for mesh reconstruction was proposed by Kato et al. [19] to approximate the gradient of pixel intensity with respect to mesh vertices. By using [19], Kanazawa et al. [18] strive to reconstruct category-specific mesh from image collections without relying on 3D ground-truth models. Apart from rasterization-based rendering, Li et al. [23] introduce a differentiable ray tracer to realize secondary rendering effects in a deep neural network.

In this paper, we focus on exploring a general differentiable framework for rasterization-based rendering. Unlike Neural 3D Mesh Renderer [19], which approximates the discrete rasterization operation with a straightforward linear function, our approach is capable to provide the estimation of rendering derivative with significantly higher accuracy.

Single-view 3D reconstruction. Image based 3D reconstruction is a long-standing problem in computer vision. Single image based reconstruction problem is especially challenging due to the mismatch between the scarcity of input and the redundancy of the plausible solutions. Recent

advances in machine learning address this issue by learning the priors of 3D properties, such as shape, reflectance or illumination [2, 4, 44] to reduce the searching space. Before the advent of differentiable renderer, a majority of prior works use supervised deep learning approaches, which seek to learn the nonlinear mapping between the input image and 3D model parameters [47, 52, 55, 42, 49] from labeled ground-truth data. To simplify the learning problem, some works reconstruct 3D shape via predicting intermediate 2.5D representations, such as depth map [43, 7, 25], visual hull [32], implicit field [15], displacement map [16] or normal map [1, 36, 50]. When considering reconstructing 3D shape, voxel-based representation has received most attention [51, 56, 48] due to its simplicity of regular structure and compatibility with convolutional neural network. However, volumetric representation is constrained by its resolution due to the data sparsity and high computational cost. Hence, recent progress on supervised learning has explored the avenue of reconstructing mesh [49, 12, 35] or point cloud [8] directly from a single image.

Comparing to supervised learning, unsupervised 3D reconstruction is becoming increasingly important as collecting ground-truth 3D models is much more difficult than labeling 2D images. Perspective transformer nets [53] propose an encoder-decoder network which learns 3D shape from silhouette images in an unsupervised fashion. The key to their approach is adding a projection transformation as a self-supervised loss for regularizing the voxel generation. Though our geometry reconstruction is also based on silhouette images, we use mesh representation which is much more computationally efficient and can reconstruct geometry with much higher precision compared to the volumetric representation in [53].

3. Soft Rasterizer

The main obstacle that impedes the standard graphics renderer from being differentiable is the discrete sampling operation, which is also named *rasterization*, that converts a continuous vector graphics into a raster image. In particular, after projecting the mesh triangles onto the screen space, standard rasterization technique fills each pixel with the color from the nearest triangle which covers that pixel. However, the color intensity of an image is the result of complex interplay between a variety of factors, including the lighting condition, viewing direction, reflectance property and the intrinsic texture of the rendered object, most of which are entirely independent from the 3D shape of the target object. Though one can infer fine surface details from the shading cues, special care has to be taken to decompose shading from the reflectance layers. Therefore, leveraging color information for 3D geometry reconstruction may unnecessarily complicate the problem especially when the target object only consists of smooth surfaces. As a pioneering

attempt for reconstructing general objects, our work only focuses on synthesizing silhouettes, which are solely determined by the 3D geometry of the object.

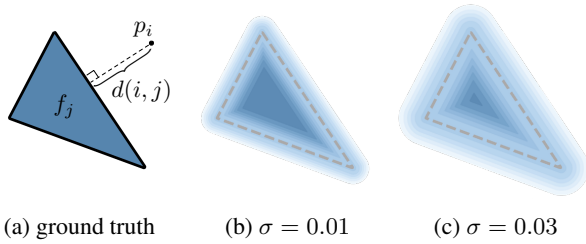


Figure 3: Example probability maps of a single triangle. (a): definition of pixel-to-triangle distance; (b) and (c): probability maps generated with different σ .

Unlike color image, the silhouette image is a binary mask where a pixel is labeled as solid as long as it is covered by any triangle. To differentiate such discrete operation, we propose to formulate it as a probabilistic procedure. In particular, instead of viewing sampling as a deterministic event, we assume that each triangle face can potentially cover a specific pixel with certain probability. Such probability distribution is highly related with the distance $d(i, j)$ between the specified pixel p_i and the triangle f_j (Figure 3). The closer p_i is to the center of f_j , the more likely p_i is covered by f_j . Towards this end, we encode the probabilistic “contribution” of triangle f_j to all image pixels in the form of *probability map*, which is denoted as D_j . The value at the i -th pixel of D_j encodes the probability of f_j covers the corresponding pixel in the final rendered image. After the probability maps $\{D_j\}$ of all triangles are obtained, we approximate the rasterization result by fusing $\{D_j\}$ with a specially-designed aggregation function $\mathcal{A}(\cdot)$. We describe the details of computing probability maps $\{D_j\}$ and aggregation function $\mathcal{A}(\cdot)$ in the following sections.

3.1. Probability Map Computation

The probability map D_j of each face f_j has the same resolution ($h \times w$) with the output silhouette image \hat{S} . As discussed before, when computing D_j , the region that is closer to the triangle center, especially those enclosed by f_j , shall receive higher weight in a properly designed probability distribution. In contrast, the probability intensity of the pixels that are outside f_j should drop fast as their distance to f_j increases. It is easy to observe that such probability distribution is closely related to the distance field with respect to the boundary of the triangle f_j . To this end, we propose the formulation of D_j as follows:

$$D_j^i = \text{sigmoid}(\delta_{ij} \cdot \frac{d^2(i, j)}{\sigma}), \quad (1)$$

where D_j^i is the probability value at the i -th pixel p_i

(scan line order) of D_j ; $d(i, j)$ returns the shortest distance from p_i to the edges of f_j (see Figure 3(a)); σ is a positive hyperparameter that controls the sharpness of the probability distribution while δ_{ij} is a signed indicator whose response depends on the relative position between p_i and f_j :

$$\delta_{ij} = \begin{cases} +1 & \text{if } p_i \in f_j \\ -1 & \text{otherwise.} \end{cases}$$

Intuitively, by using the *sigmoid* function, Equation 1 generates a normalized output staying within the interval $(0, 1)$. In addition, the introduction of the signed indicator maps pixels inside and outside f_j to the probability distribution of $(0.5, 1)$ and $(0, 0.5)$ respectively. Figure 3 shows D_j of a particular triangle with different configurations of σ . As shown in the results, smaller σ leads to sharper probability distribution while larger σ tends to generate more blurry outcome. As $\sigma \rightarrow 0$, the resulting probability field converges to the exact silhouette of the triangle.

It is worth noting that before computing the pixel-to-triangle distance $d(i, j)$, we first normalize the pixel coordinates into $[-1, 1]$. This helps factor out the bias introduced by different image resolutions. Though it is possible to directly use $d(i, j)$ in the computation of D_j , in practice, we found $d^2(i, j)$ works better as it introduces a sharper distribution of the probability field.

3.2. Aggregate Function

As the probability map D_j of each triangle face is computed in an independent manner, there remains a key step to aggregate them to obtain the final rendering result. To achieve this goal, we first analyze the working principal of standard rendering pipeline. The standard rasterizer synthesizes silhouette image by following a strict logical *or* operation. In particular, a pixel that is covered by any triangle on the image plane will be rendered as the interior of the object in the output silhouette image. As our proposed probability formulation has emphasized the inner pixels enclosed by each triangle with higher weight – their probability values are closer to 1 – we approximate the logical *or* operator by proposing the following aggregation function:

$$\hat{S}^i = \mathcal{A}(\{D_j\}) = 1 - \prod_j^N (1 - D_j^i), \quad (2)$$

where \hat{S}^i represents the i -th pixel in the final silhouette image and N is the number of total mesh triangles. Intuitively, when there exists a D_j^i whose value is 1, then \hat{S}^i will be marked as 1 regardless the probability value of other probability maps at this pixel location. On the other hand, \hat{S}^i will receive 0 only when all $\{D_j^i\}$ are zeros.

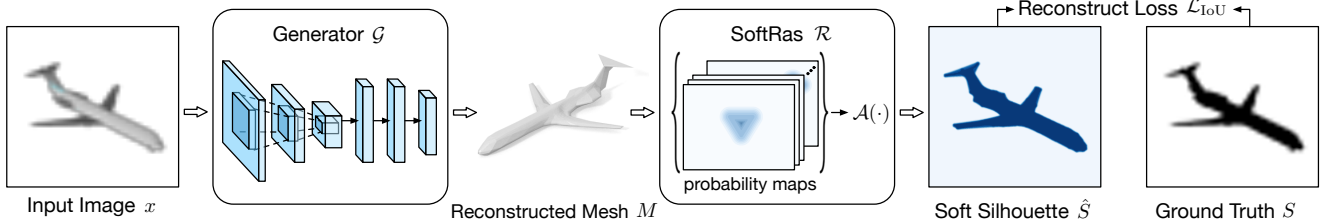


Figure 4: Our pipeline for unsupervised single-image 3D mesh reconstruction: (1) mesh generator \mathcal{G} takes an input image x and outputs the displacement vector $\mathcal{G}(x)$, which is added to a template model to obtain the reconstructed mesh M ; (2) SoftRas layer \mathcal{R} transforms triangles in M into probability maps and computes soft silhouette \hat{S} using the aggregation function $\mathcal{A}(\cdot)$. IoU loss is then applied to minimize the discrepancy between \hat{S} and ground truth S .

Figure 4 demonstrates the generated silhouette using our soft rasterizer with $\sigma = 3 \times 10^{-5}$. As shown in the result, SoftRas is able to faithfully approximate the ground-truth silhouette without losing fine details. However, unlike the standard rasterizer, which includes discrete non-differentiable operations, our SoftRas is entirely differentiable thanks to its continuous definition.

4. Unsupervised Mesh Reconstruction

To demonstrate the effectiveness of the proposed soft rasterizer, we incorporate it into a simple mesh generator for the task of image-based 3D reconstruction. In particular, we propose an end-to-end deep learning framework that takes a single color image x as input and reconstructs its corresponding 3D mesh model M without requiring the camera parameters. As illustrated in the framework overview in Figure 4, our system mainly consists of two parts: one mesh generator that deforms a template sphere mesh to the desired 3D model and a soft rasterizer layer that renders the silhouette image of the reconstructed mesh.

4.1. Mesh Generator

Inspired by the state-of-the-art mesh learning approaches [19, 49], we leverage a similar idea of synthesizing 3D model by deforming a template mesh. To validate the performance of our proposed soft rasterizer, we employ an encoder-decoder architecture which is nearly identical to that of [19]. In particular, the mesh generator consumes a 4-channel color image, in which the last channel specifies the object’s silhouette mask, and predicts per-vertex displacement vectors that deform the template mesh to the desired shape. We use the same template mesh – a sphere model – with Neural 3D Mesh Renderer [19].

The training of our network does not require any 3D ground truth. Specifically, our network is only trained with multi-view silhouettes of the objects collected in the training set. Thanks to the differentiability of soft rasterizer, the learning of mesh generator is directly supervised by the rendering loss computed from the difference between the ren-

dered and the ground-truth silhouettes.

Losses. As object silhouette is represented in the form of binary mask, to evaluate the accuracy of our prediction, we adopt the intersection over union (IoU) loss \mathcal{L}_{IoU} for a proper measurement. In addition, to enforce the generator produces smooth and appealing results, we impose two additional geometry regularizer to constrain the property of output shape. We provide the details of losses as follows.

IoU Loss. We denote \hat{S} and S as the binary masks of the reconstructed and ground-truth silhouette respectively and define \otimes and \oplus be the operators that performs element-wise product and sum respectively. Therefore our IoU loss can be represented as:

$$\mathcal{L}_{IoU} = 1 - \frac{\|\hat{S} \otimes S\|_1}{\|\hat{S} \oplus S - \hat{S} \otimes S\|_1} \quad (3)$$

Laplacian Loss. A simple IoU loss only focuses on pushing the mesh projection to be consistent with the true silhouette but could lead to strongly deformed mesh due to the priority to favor local consistency. To prevent the vertices from moving too freely, we add a Laplacian term to regularize the geometry. Let M be the output triangular mesh with n vertices. Each vertex $i \in M$ is denoted as $v_i = (x_i, y_i, z_i)$. We first define the laplacian coordinate for v_i as the difference between the coordinates of v_i and the center of mass of its immediate neighbors: $\delta_i = v_i - \frac{1}{\|N(i)\|} \sum_{j \in N(i)} v_j$. The laplacian loss is defined as:

$$\mathcal{L}_{lap} = \sum_i \|\delta_i\|_2^2 \quad (4)$$

Flattening Loss. In addition to laplacian loss, we also employ a flattening loss [19] to encourage adjacent triangle faces to have similar normal directions. Empirically, we found the introduced flattening loss can further smooth the surface and prevent self-intersections. To calculate the flattening loss, we set θ_i to be the angle between the faces that have the common edge e_i . Therefore, the flattening loss can be defined as:

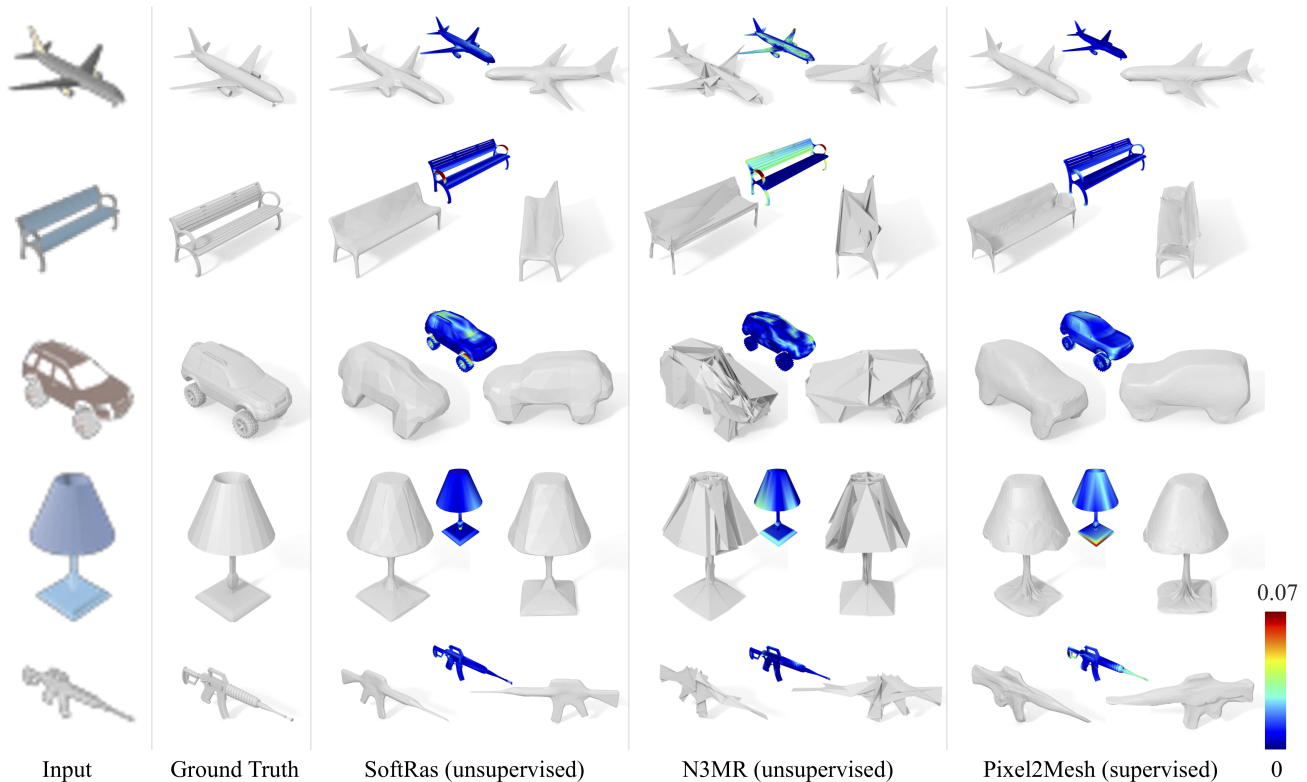


Figure 5: 3D mesh reconstruction from a single image. From left to right, we show input image, ground truth, the results of our method (SoftRas), Neural Mesh Renderer [19] and Pixel2mesh [49], all visualized from 2 different views. Along with the results, we also visualize scan-to-mesh distances measured from ground truth to reconstructed mesh.

Category	Airplane	Bench	Dresser	Car	Chair	Display	Lamp
retrieval [53]	0.5564	0.4875	0.5713	0.6519	0.3512	0.3958	0.2905
voxel-based [53]	0.5556	0.4924	0.6823	0.7123	0.4494	0.5395	0.4223
N3MR [19]	0.6172	0.4998	0.7143	0.7095	0.4990	0.5831	0.4126
SoftRas (ours)	0.6419	0.5080	0.7116	0.7697	0.5270	0.6156	0.4628
Category	Loudspeaker	Rifle	Sofa	Table	Phone	Vessel	Mean
retrieval [53]	0.4600	0.5133	0.5314	0.3097	0.6696	0.4078	0.4766
voxel-based [53]	0.5868	0.5987	0.6221	0.4938	0.7504	0.5507	0.5736
N3MR [19]	0.6536	0.6322	0.6735	0.4829	0.7777	0.5645	0.6015
SoftRas (ours)	0.6654	0.6811	0.6878	0.4487	0.7895	0.5953	0.6234

Table 1: Comparison of mean IoU with other unsupervised 3D reconstruction methods on 13 categories of ShapeNet datasets.

$$\mathcal{L}_{fl} = \sum_{\theta_i \in e_i} (\cos \theta_i + 1)^2 \quad (5)$$

where \mathcal{L}_{fl} will reach its minimum value if all adjacent faces stay on the same plane. The final loss is a weighted sum of the three particular losses:

$$\mathcal{L} = \mathcal{L}_{IoU} + \lambda \mathcal{L}_{lap} + \mu \mathcal{L}_{fl} \quad (6)$$

Color Reconstruction. Unlike vertex position, the vertex color can naturally receive gradients back propagated from

the image loss. Thanks to the proposed differentiable rasterizer, we are able to recover both 3D geometry and the accompanied vertex color in an end-to-end manner. In particular, we leverage the l_2 loss to measure the difference between the projection of recovered colorful mesh and the input image. We show the results of colorized reconstruction in Section 5.2.

5. Experiments

In this section, we perform an extensive evaluation on our framework. We first provide the details of our experimental setups and then demonstrate a variety of results and ablation studies. We also include video result and more vi-

sual evaluations in the *supplemental materials*. The code and data will be released upon publication.

5.1. Experimental Setup

Datasets. We use the dataset provided by [19]. In particular, the dataset contains 13 categories of objects belonging to ShapeNet [5], a large-scale 3D model collection containing about 50k unique meshes from 55 categories. Each object is rendered with 24 different views with image resolution of 64×64 . To ensure fair comparison, we employ the same train/validate/test split as in [19, 53].

Evaluation Metrics. For quantitative evaluation, we adopt the standard reconstruction metric, 3D intersection over union (IoU), to compare with baseline methods. On the other hand, we agree with Pixel2Mesh [49] that the commonly used metric may not be able to thoroughly reflect the quality of geometry reconstruction, such as smoothness and continuity of the surface. Therefore, we wish to emphasize the importance of visual quality, which is important in real applications.

Implementation Details. We use similar mesh generation network with [19], which is implemented as an encoder-decoder architecture. The encoder network consists of 3 convolutional layers with kernel size of 5×5 and channels of 64, 128, 256, followed by 3 fully connected layers with hidden layer size of 1024 and 1024. In particular, we apply batch normalization [17] and ReLU activation [21] after each convolutional layer. The decoder transforms a 512-dimensional latent code into a displacement vector of length 1926 (coordinates of 642 vertices) by using 3 fully connected layers with hidden size of 1024 and 2048. Our network is trained with Adam optimizer [20] with $\alpha = 0.0001$, $\beta_1 = 0.9$ and $\beta_2 = 0.999$. In our implementation, we set $\sigma = 3 \times 10^{-5}$ (Equation 1), $\lambda = 0.01$ and $\mu = 0.001$ (Equation 6) across all experiments unless otherwise specified. We train the network with batch size of 64 with multi-view inputs and implement it using PyTorch¹. The code and data will be released upon publication.

5.2. Qualitative Results

Single-view Mesh Reconstruction. We compare the qualitative results of our approach with that of the state-of-the-art supervised [49] and unsupervised [19] mesh reconstruction approaches in Figure 5. Though Neural 3D Mesh Renderer (N3MR) [19] is able to recover the rough shape, the mesh surface is discontinuous and suffers from a considerable amount of self intersections. In contrast, our method can faithfully reconstruct fine details of the object, such as the empennage and engines of airplane and



(a) Input image (b) Reconstruction results

Figure 6: Results of colored mesh reconstruction.

the barrel of rifle, while ensuring smoothness of the generated surface. Though trained in an entirely unsupervised manner, our approach achieves comparable results with the supervised method Pixel2Mesh [49]. For objects that are not genus-0, e.g. the bench in the second row of Figure 5, Pixel2Mesh generates better results than ours (see the armrest). The reason is that as our method can only generate genus-0 surface, synthesizing the armrest will lead to large 2D IoU loss. In contrast, Pixel2Mesh employs 3D Chamfer distance as loss metric which could strongly penalize the missing of armrest in the reconstructed model. However, in some cases, our approach can generate even smoother and sharper results than that of [49], e.g. the lamp base, the engine of airplane and the rifle. Scan-to-mesh distance visualization also shows our results achieve comparable accuracy, in terms of tightness between reconstructed meshes and ground truth.

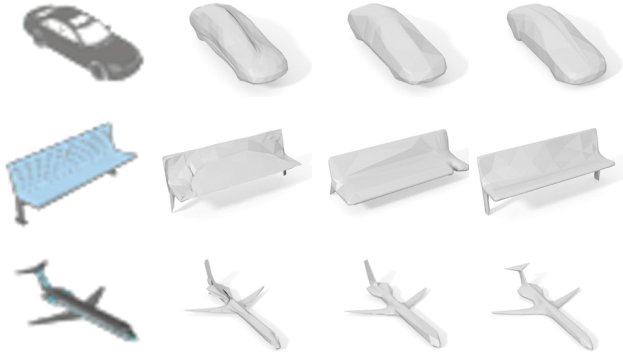
Color Reconstruction. Our method is also capable to recover per-vertex color of the generated mesh based on the input image. Figure 6 presents the colored reconstruction from a single image. Though the resolution of the input image is rather low (64×64), our approach is still able to achieve sharp reconstruction and accurately restore the detailed vertex colors, e.g. the blue color of the airplane tail.

5.3. Quantitative Evaluations

We show the comparisons on 3D IoU score with different approaches. Table 1 lists the statistics for all categories. As seen in Table 1, our mean score surpasses the state-of-the-art N3MR by more than 2.1%. In addition, our approach also achieves the top accuracy for most of the categories. Our score for the table category is slightly worse than PTN [53] and N3MR. The main reason is that most of our reconstructed tables contain a 30° embossment over the main flat surface (see Figure 8 (b)). We found all training images are rendered from the viewpoints at 30° on the axis of elevation. This would lead to an ambiguity of the intended structure as our reconstructed model in fact can generate silhouette that matches the input image well. We provide an ablation anal-

¹<https://pytorch.org/>

ysis in Section 5.4 to further validate our model with more comprehensive training views.



(a) Input image (b) w/o \mathcal{L}_{fl} (c) w/o \mathcal{L}_{lap} (d) Full model

Figure 7: Ablation study of different loss terms.

5.4. Ablation Study

In this section, we conduct controlled experiments to validate the importance of different components.

Loss Terms. We first investigate the influence of the two losses, \mathcal{L}_{lap} and \mathcal{L}_{fl} , that regularize the geometry property of the generated mesh models. Figure 7 shows the results of selectively dropping one of the losses. As seen from the comparisons, removing the Laplacian loss \mathcal{L}_{lap} would lead to less smooth surface, e.g. the head of airplane, or even discontinuities, e.g. the hole in the bench seat. Dropping off the flattening loss \mathcal{L}_{fl} would severely impair the smoothness of surface and causes intersecting geometry, e.g. the bench back and the tail part of airplane. However, when the losses are both present, our full model does not suffer from any of the problems, indicating both of the components are necessary for our final performance.



(a) Input image (b) 24 views (c) 120 views (d) Ground Truth

Figure 8: Comparison of results reconstructed from different numbers of training views. With more training views, our approach can achieve reconstruction with significantly higher accuracy.



(a) Input image (b) Pixel2Mesh (c) SoftRas (ours)

Figure 9: Comparisons of 3D reconstruction from real images. Our results are shown in two different views.

Training with More Views. As discussed in Section 5.3, the existing dataset only contains limited biased views, resulting in a large degree of ambiguity in the reconstructed models. To evaluate the full capability of our model, we render the existing models with more comprehensive views. In particular, the new training images are rendered from 120 viewpoints, sampled from 5 elevation and 24 azimuth angles. As shown in Figure 8, by training with more views, our model is capable to generate results much closer to the ground truth. In particular, the embossment of the table model has been completely removed in the new results, indicating the effectiveness of the silhouette supervision obtained from our SoftRas layer.

Reconstruction from Real Image. We further evaluate our approach on real images and compare with Pixel2Mesh [49]. Here we employ the model trained on 120 views as proposed in experiment above. As demonstrated in Figure 2 (right) and Figure 9, though only trained on synthetic data, our model generalizes well to real images in novel views with faithful reconstruction of fine details, e.g. the tail fins of the fighter aircraft. While for most examples, our unsupervised approach produces comparable results to the supervised method, Pixel2Mesh, we found many cases where our technique can significantly outperform theirs, especially for real world images (see Figure 9 (b) and (c)).

6. Discussion and Future Work

In this paper, we have presented the first non-parametric differentiable rasterizer (SoftRas) that enables unsupervised learning for high-quality mesh reconstruction from a single image. We demonstrate that it is possible to properly approximate the forward pass of the discrete rasterization with a differentiable framework. While many previous works like N3MR [19] seek to provide approximated gradient in the backward propagation but using standard rasterizer in the forward pass, we believe that the consistency between the forward and backward propagations is the key to achieve superior performance. In addition, we found that proper choice of regularizers plays an important role for producing visually appealing geometry. Experiments have shown that

our unsupervised approach achieves comparable and in certain cases, even better results to state-of-the-art supervised solutions.

Limitations and future work. As SoftRAS only provides silhouette based supervision, ambiguity may arise in our reconstruction when only limited views are available. Such ambiguity is pronounced when there exists a large planar surface in the object (Figure 8(b)). However, it is possible to resolve this issue by training our model with more comprehensive views (Figure 8(c)). It would be an interesting future avenue to study the gradient of pixel colors with respect to mesh vertices such that the shading cues can be considered for reconstruction.

Acknowledgements

This work was supported in part by the ONR YIP grant N00014-17-S-FO14, the CONIX Research Center, one of six centers in JUMP, a Semiconductor Research Corporation (SRC) program sponsored by DARPA, the Andrew and Erna Viterbi Early Career Chair, the U.S. Army Research Laboratory (ARL) under contract number W911NF-14-D-0005, Adobe, and Sony. The content of the information does not necessarily reflect the position or the policy of the Government, and no official endorsement should be inferred.

References

- [1] A. Bansal, B. Russell, and A. Gupta. Marr revisited: 2d-3d alignment via surface normal prediction. In *Proceedings of the IEEE conference on computer vision and pattern recognition*, pages 5965–5974, 2016.
- [2] J. T. Barron and J. Malik. Shape, illumination, and reflectance from shading. *IEEE transactions on pattern analysis and machine intelligence*, 37(8):1670–1687, 2015.
- [3] B. G. Baumgart. Geometric modeling for computer vision. Technical report, STANFORD UNIV CA DEPT OF COMPUTER SCIENCE, 1974.
- [4] V. Blanz and T. Vetter. A morphable model for the synthesis of 3d faces. In *Proceedings of the 26th annual conference on Computer graphics and interactive techniques*, pages 187–194. ACM Press/Addison-Wesley Publishing Co., 1999.
- [5] A. X. Chang, T. Funkhouser, L. Guibas, P. Hanrahan, Q. Huang, Z. Li, S. Savarese, M. Savva, S. Song, H. Su, et al. Shapenet: An information-rich 3d model repository. *arXiv preprint arXiv:1512.03012*, 2015.
- [6] V. Deschaintre, M. Aittala, F. Durand, G. Drettakis, and A. Bousseau. Single-image svbrdf capture with a rendering-aware deep network. *ACM Transactions on Graphics (TOG)*, 37(4):128, 2018.
- [7] D. Eigen and R. Fergus. Predicting depth, surface normals and semantic labels with a common multi-scale convolutional architecture. In *Proceedings of the IEEE International Conference on Computer Vision*, pages 2650–2658, 2015.
- [8] H. Fan, H. Su, and L. J. Guibas. A point set generation network for 3d object reconstruction from a single image. In *CVPR*, volume 2, page 6, 2017.
- [9] K. Genova, F. Cole, A. Maschinot, A. Sarna, D. Vlasic, and W. T. Freeman. Unsupervised training for 3d morphable model regression. In *Proceedings of the IEEE Conference on Computer Vision and Pattern Recognition*, pages 8377–8386, 2018.
- [10] I. Gkioulekas, A. Levin, and T. Zickler. An evaluation of computational imaging techniques for heterogeneous inverse scattering. In *European Conference on Computer Vision*, pages 685–701. Springer, 2016.
- [11] I. Gkioulekas, S. Zhao, K. Bala, T. Zickler, and A. Levin. Inverse volume rendering with material dictionaries. *ACM Transactions on Graphics (TOG)*, 32(6):162, 2013.
- [12] T. Groueix, M. Fisher, V. G. Kim, B. Russell, and M. Aubry. AtlasNet: A Papier-Mâché Approach to Learning 3D Surface Generation. In *Proceedings IEEE Conf. on Computer Vision and Pattern Recognition (CVPR)*, 2018.
- [13] K. He, X. Zhang, S. Ren, and J. Sun. Deep residual learning for image recognition. In *Proceedings of the IEEE conference on computer vision and pattern recognition*, pages 770–778, 2016.
- [14] D. Hoiem, A. A. Efros, and M. Hebert. Automatic photo pop-up. In *ACM transactions on graphics (TOG)*, volume 24, pages 577–584. ACM, 2005.
- [15] Z. Huang, T. Li, W. Chen, Y. Zhao, J. Xing, C. LeGendre, L. Luo, C. Ma, and H. Li. Deep volumetric video from very sparse multi-view performance capture. In *European Conference on Computer Vision*, pages 351–369. Springer, 2018.
- [16] L. Huynh, W. Chen, S. Saito, J. Xing, K. Nagano, A. Jones, P. Debevec, and H. Li. Mesoscopic facial geometry inference using deep neural networks. In *Proceedings of the IEEE Conference on Computer Vision and Pattern Recognition*, pages 8407–8416, 2018.
- [17] S. Ioffe and C. Szegedy. Batch normalization: Accelerating deep network training by reducing internal covariate shift. *arXiv preprint arXiv:1502.03167*, 2015.
- [18] A. Kanazawa, S. Tulsiani, A. A. Efros, and J. Malik. Learning category-specific mesh reconstruction from image collections. *arXiv preprint arXiv:1803.07549*, 2018.
- [19] H. Kato, Y. Ushiku, and T. Harada. Neural 3d mesh renderer. In *Proceedings of the IEEE Conference on Computer Vision and Pattern Recognition*, pages 3907–3916, 2018.
- [20] D. P. Kingma and J. Ba. Adam: A method for stochastic optimization. *arXiv preprint arXiv:1412.6980*, 2014.
- [21] A. Krizhevsky, I. Sutskever, and G. E. Hinton. Imagenet classification with deep convolutional neural networks. In *Advances in neural information processing systems*, pages 1097–1105, 2012.
- [22] A. Kundu, Y. Li, and J. M. Rehg. 3d-rcnn: Instance-level 3d object reconstruction via render-and-compare. In *Proceedings of the IEEE Conference on Computer Vision and Pattern Recognition*, pages 3559–3568, 2018.
- [23] T.-M. Li, M. Aittala, F. Durand, and J. Lehtinen. Differentiable monte carlo ray tracing through edge sampling. *ACM Trans. Graph. (Proc. SIGGRAPH Asia)*, 37(6):222:1–222:11, 2018.
- [24] G. Lin, C. Shen, A. Van Den Hengel, and I. Reid. Efficient piecewise training of deep structured models for semantic segmentation. In *Proceedings of the IEEE Conference on Computer Vision and Pattern Recognition*, pages 3194–3203, 2016.
- [25] F. Liu, C. Shen, G. Lin, and I. D. Reid. Learning depth from single monocular images using deep convolutional neural fields. *IEEE Trans. Pattern Anal. Mach. Intell.*, 38(10):2024–2039, 2016.

- [26] G. Liu, D. Ceylan, E. Yumer, J. Yang, and J.-M. Lien. Material editing using a physically based rendering network. In *Computer Vision (ICCV), 2017 IEEE International Conference on*, pages 2280–2288. IEEE, 2017.
- [27] M. M. Loper and M. J. Black. Opendr: An approximate differentiable renderer. In *European Conference on Computer Vision*, pages 154–169. Springer, 2014.
- [28] D. G. Lowe. Three-dimensional object recognition from single two-dimensional images. *Artificial intelligence*, 31(3):355–395, 1987.
- [29] V. K. Mansinghka, T. D. Kulkarni, Y. N. Perov, and J. Tenenbaum. Approximate bayesian image interpretation using generative probabilistic graphics programs. In *Advances in Neural Information Processing Systems*, pages 1520–1528, 2013.
- [30] D. Marr. *Vision: A computational investigation into the human representation and processing of visual information*. MIT press. Cambridge, Massachusetts, 1982.
- [31] O. Nalbach, E. Arabadzhiyska, D. Mehta, H.-P. Seidel, and T. Ritschel. Deep shading: convolutional neural networks for screen space shading. In *Computer graphics forum*, volume 36, pages 65–78. Wiley Online Library, 2017.
- [32] R. Natsume, S. Saito, Z. Huang, W. Chen, C. Ma, H. Li, and S. Morishima. Siclope: Silhouette-based clothed people. *arXiv preprint arXiv:1901.00049*, 2018.
- [33] T. Nguyen-Phuoc, C. Li, S. Balaban, and Y. Yang. Rendernet: A deep convolutional network for differentiable rendering from 3d shapes. *arXiv preprint arXiv:1806.06575*, 2018.
- [34] G. Patow and X. Pueyo. A survey of inverse rendering problems. In *Computer graphics forum*, volume 22, pages 663–687. Wiley Online Library, 2003.
- [35] A. Pumarola, A. Agudo, L. Porzi, A. Sanfeliu, V. Lepetit, and F. Moreno-Noguer. Geometry-aware network for non-rigid shape prediction from a single view. In *Proceedings of the IEEE Conference on Computer Vision and Pattern Recognition*, pages 4681–4690, 2018.
- [36] X. Qi, R. Liao, Z. Liu, R. Urtasun, and J. Jia. Geonet: Geometric neural network for joint depth and surface normal estimation. In *Proceedings of the IEEE Conference on Computer Vision and Pattern Recognition*, pages 283–291, 2018.
- [37] S. Ren, K. He, R. Girshick, and J. Sun. Faster r-cnn: Towards real-time object detection with region proposal networks. In *Advances in neural information processing systems*, pages 91–99, 2015.
- [38] D. J. Rezende, S. A. Eslami, S. Mohamed, P. Battaglia, M. Jaderberg, and N. Heess. Unsupervised learning of 3d structure from images. In *Advances in Neural Information Processing Systems*, pages 4996–5004, 2016.
- [39] E. Richardson, M. Sela, R. Or-El, and R. Kimmel. Learning detailed face reconstruction from a single image. In *Computer Vision and Pattern Recognition (CVPR), 2017 IEEE Conference on*, pages 5553–5562. IEEE, 2017.
- [40] L. G. Roberts. *Machine perception of three-dimensional solids*. PhD thesis, Massachusetts Institute of Technology, 1963.
- [41] A. Saxena, M. Sun, and A. Y. Ng. Make3d: Learning 3d scene structure from a single still image. *IEEE transactions on pattern analysis and machine intelligence*, 31(5):824–840, 2009.
- [42] S. Sengupta, A. Kanazawa, C. D. Castillo, and D. W. Jacobs. Sfsnet: learning shape, reflectance and illuminance of faces in the wild. In *Proceedings of the IEEE Conference on Computer Vision and Pattern Recognition (CVPR)*, pages 6296–6305, 2018.
- [43] E. Shelhamer, J. T. Barron, and T. Darrell. Scene intrinsics and depth from a single image. In *Proceedings of the IEEE International Conference on Computer Vision Workshops*, pages 37–44, 2015.
- [44] J. Shi, Y. Dong, H. Su, and X. Y. Stella. Learning non-lambertian object intrinsics across shapenet categories. In *Computer Vision and Pattern Recognition (CVPR), 2017 IEEE Conference on*, pages 5844–5853. IEEE, 2017.
- [45] A. Tewari, M. Zollhöfer, P. Garrido, F. Bernard, H. Kim, P. Pérez, and C. Theobalt. Self-supervised multi-level face model learning for monocular reconstruction at over 250 hz. In *Proceedings of the IEEE Conference on Computer Vision and Pattern Recognition*, pages 2549–2559, 2018.
- [46] A. Tewari, M. Zollhöfer, H. Kim, P. Garrido, F. Bernard, P. Pérez, and C. Theobalt. Mofa: Model-based deep convolutional face autoencoder for unsupervised monocular reconstruction. In *The IEEE International Conference on Computer Vision (ICCV)*, volume 2, page 5, 2017.
- [47] L. Tran and X. Liu. Nonlinear 3d face morphable model. *arXiv preprint arXiv:1804.03786*, 2018.
- [48] S. Tulsiani, T. Zhou, A. A. Efros, and J. Malik. Multi-view supervision for single-view reconstruction via differentiable ray consistency. In *CVPR*, volume 1, page 3, 2017.
- [49] N. Wang, Y. Zhang, Z. Li, Y. Fu, W. Liu, and Y.-G. Jiang. Pixel2mesh: Generating 3d mesh models from single rgb images. In *ECCV*, 2018.
- [50] X. Wang, D. Fouhey, and A. Gupta. Designing deep networks for surface normal estimation. In *Proceedings of the IEEE Conference on Computer Vision and Pattern Recognition*, pages 539–547, 2015.
- [51] J. Wu, Y. Wang, T. Xue, X. Sun, B. Freeman, and J. Tenenbaum. Marrnet: 3d shape reconstruction via 2.5 d sketches. In *Advances in neural information processing systems*, pages 540–550, 2017.
- [52] S. Yamaguchi, S. Saito, K. Nagano, Y. Zhao, W. Chen, K. Olszewski, S. Morishima, and H. Li. High-fidelity facial reflectance and geometry inference from an unconstrained image. *ACM Transactions on Graphics (TOG)*, 37(4):162, 2018.
- [53] X. Yan, J. Yang, E. Yumer, Y. Guo, and H. Lee. Perspective transformer nets: Learning single-view 3d object reconstruction without 3d supervision. In *Advances in Neural Information Processing Systems*, pages 1696–1704, 2016.
- [54] Y. Yu, P. Debevec, J. Malik, and T. Hawkins. Inverse global illumination: Recovering reflectance models of real scenes from photographs. In *Proceedings of the 26th annual conference on Computer graphics and interactive techniques*, pages 215–224. ACM Press/Addison-Wesley Publishing Co., 1999.
- [55] Y. Zhou, L. Hu, J. Xing, W. Chen, H.-W. Kung, X. Tong, and H. Li. Single-view hair reconstruction using convolutional neural networks. *arXiv preprint arXiv:1806.07467*, 2018.
- [56] R. Zhu, H. K. Galoogahi, C. Wang, and S. Lucey. Rethinking reprojection: Closing the loop for pose-aware shape reconstruction from a single image. In *Computer Vision (ICCV), 2017 IEEE International Conference on*, pages 57–65. IEEE, 2017.
- [57] J. Zienkiewicz, A. Davison, and S. Leutenegger. Real-time height map fusion using differentiable rendering. In *Intelligent Robots and Systems (IROS), 2016 IEEE/RSJ International Conference on*, pages 4280–4287. IEEE, 2016.